Polarizability measurements in a molecule near-field interferometer

Martin Berninger, André Stefanov, Sarayut Deachapunya, and Markus Arndt*

Fakultät für Physik der Universität Wien,
Boltzmanngasse 5, A–1090 Wien

(Dated: February 9, 2008)

We apply near-field matter-wave interferometry to determine the absolute scalar polarizability of the fullerenes C_{60} and C_{70}. A key feature of our experiment is the combination of good transmission and high spatial resolution, gained by wide molecular beams passing through sub-micron gratings. This allows to significantly facilitate the observation of field-dependent beam shifts. We thus measure the polarizability to be $\alpha = 88.9 \pm 0.9 \pm 5.1 \, \text{Å}^3$ for C_{60} and to $\alpha = 108.5 \pm 2.0 \pm 6.2 \, \text{Å}^3$ for C_{70}.

PACS numbers: 03.65.-w; 03.75.-b; 06.20.-f; 33.15.Kr; 39.20.+q

Knowing the scalar polarizability of a molecule is of importance in various areas of physics. The polarizability may provide one of several parameters in the description of molecular shapes [1]. Even for the structurally simple molecules C_{60} and C_{70}, various theoretical models have been competing with each other [2].

The molecular response to external electric fields is also the handle for slowing [3, 4, 5] cooling or trapping [6] neutral particles in switched electric fields or off-resonant laser beams.

It also turns out to be crucial for matter-wave interferometry. The van der Waals or Casimir-Polder potentials acting between the traversing molecules and the diffraction gratings have an enormous influence on the details of the interference fringes [7, 8]. And this will generally grow with the the size of the particles.

Also the small-angle scattering cross section between different molecules is related to their polarizability. And this enters, for instance, experimental considerations through the definition of the vacuum conditions which are required for avoiding collisional decoherence in interferometry [9].

Finally, precise α-measurements are also stimulated by the insight that future molecule interferometers will also exploit optical gratings [10, 11, 12]. There the polarizability is needed to determine the phase shift caused by the interaction between the induced dipole moment and the electric field of the diffracting laser beam.

Various experimental approaches are conceivable to determine α with high precision [2]. In solids or liquids, the polarizability can be obtained through a measurement of the dielectric constant and the index of refraction [1]. But in particular for the comparison with theoretical models it is desirable to get information about the isolated particles [13].

Polarizabilities of dilute molecular beams are usually characterized in Stark-deflection experiments, in which the neutral molecules are traversing a homogeneous electrostatic force field. The polarizability can then be de-

termined by measuring the lateral shift of the molecular beam due to this field. In most experiments the resulting deflections are much smaller than the width of the molecular beam profile [2] but still such experiments can typically reach an accuracy of about 10% [14]. One may also consider the use of electric field gradients to induce a longitudinal velocity shift and corresponding time-of-flight delay in a molecular fountain arrangement [15].

For atoms, very precise polarizability values were also obtained using far-field matter-wave interferometry: the atomic wave function can be coherently split and guided through two spatially separated electric fields. The different phases imprinted on the atom through the interaction between α and electric field E along the two different paths shows up as a fringe shift that can be well resolved. This allowed a very accurate determination of ground state polarizabilities for Sodium [16] and Lithium [17].

Efficient methods are also highly desirable for metrology on large molecules, in particular since their α/m-values may be significantly smaller than those of alkali atoms. The use of far-field interferometry would, however, require beam sources of very high spatial coherence. In the absence of efficient cooling and phase-space compression methods, this can only be achieved by strictly collimating the molecular beam. We have demonstrated far-field diffraction successfully in our earlier work for large carbon molecules [18] but the limited flux of almost all other large particles would prohibit such a strict spatial selection. While classical Stark deflection usually provides a high flux with a low spatial resolution, far-field interferometers trade their high-resolution in for a strongly restricted molecular transmission.

Here we report on a solution of this problem, which is based on a near-field Talbot-Lau interferometer (TLI). It combines high spatial resolution with high molecular throughput and in can be generalized to objects of arbitrary mass — in the limit of classical Moiré deflectometry.

A Talbot-Lau interferometer uses near-field wave effects, generally for the lensless imaging of periodic nanostructures [19]. It has already been described earlier in the context of atom [20, 21] and molecule [8, 22] interferometry. In our present apparatus we employ a TLI composed of three gold gratings with a grating period of g=991 nm

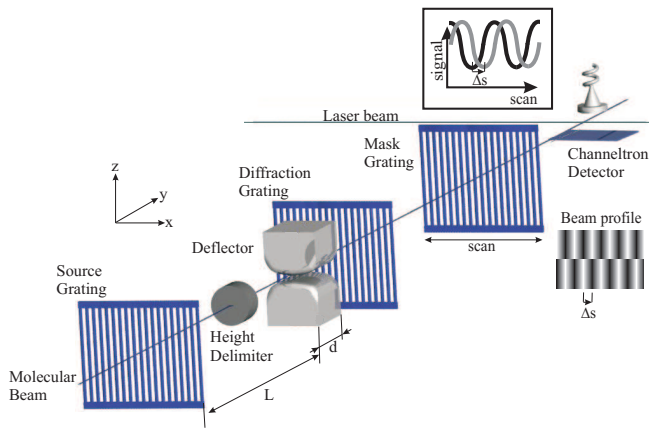*Electronic address: markus.arndt@univie.ac.at

FIG. 1: Experimental set-up: The three gratings are used for coherence preparation, diffraction and detection. Path-dependent matter-wave phase shifts in the external field lead to a beam deflection at the position of the mask grating. The lateral shift Δs of the interference fringes at the detector is directly proportional to the scalar molecular polarizability α.

with a deflection voltage of $0\,\mathrm{kV}$ and $6\,\mathrm{kV}$. The field-dependent shifts can be nicely resolved and measured with high accuracy. In order to obtain additional statistical information and to assess the accuracy of the various contributing parameters, we repeat the measurements for different velocity distributions and for different deflection voltages. We employ a gravitational velocity selec-
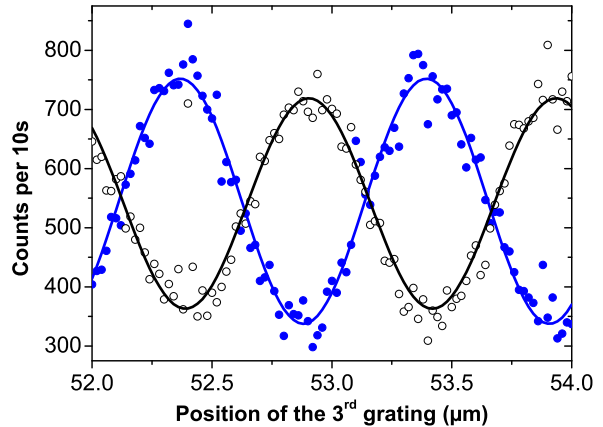

FIG. 2: Deflection of a C_{60} beam with $\bar{v} = 117\,\mathrm{m/s}$ and $\sigma_v = 8\,\%$. A phase shift of $\Delta\phi = \pi$ is obtained at a voltage of $6\,\mathrm{kV}$ (full circles). The open circles represent the reference at U=0 kV.

and slit openings of about $450\,\mathrm{nm}$ width.

The first grating prepares the required spatial coherence to obtain matter wave diffraction at the second grating, which then results in a regular molecular density pattern, immediately in front of the mask grating. The interference fringes, whose periodicity equals the gratings constant, can be revealed by scanning the third grating laterally. The resulting modulation of the molecular flux behind this setup allows to visualize the molecular nano-fringe system. The molecular beam width in a TL-interferometer may be wider than $1\,\mathrm{mm}$, allowing a high throughput of molecules while the resolution of the fringe system can be better than $15\,\mathrm{nm}$.

We now insert an electrostatic deflector into the TLI (see Fig. 1), which creates a homogeneous force field $\mathbf{F} = \alpha(\mathbf{E}\nabla E)$ changing the momentum of the molecules in proportion to the applied electric field $\mathbf{E}$, its gradient $\nabla\mathbf{E}$ and to the polarizability α. In the proper quantum picture, the electric field adds a path-dependent phase shift on the molecular matter wave. In both descriptions, classical and quantum, we obtain a fringe shift:

$$\Delta s_x(\alpha, v) = \alpha \frac{(\mathbf{E}\nabla)E_x}{m} \frac{d}{v^2}\left(\frac{d}{2} + L\right) \qquad (1)$$

where m corresponds to the molecular mass, v the velocity along the direction of the beam and L the distance between the source grating and the deflector. The front edge of the deflector (length d) is positioned at $L = (26.6 \pm 0.1)\,\mathrm{cm}$ behind the first grating. The deflector provides a constant force with deviations of 0.5% along the x-axis over the entire molecular beam diameter.

Two interference recordings at two different deflection voltages would be sufficient to determine the molecular polarizability, if all parameters were known with arbitrary precision. Figure 2 shows a fringe system of C_{60}

tion [8, 23] and chose the velocity by moving the source to its appropriate vertical position. An interference pattern is then recorded by displacing the third grating in steps of $20\,\mathrm{nm}$ over about three fringe periods and by repeating this scan for all voltages within 3–$15\,\mathrm{kV}$ in steps of $1\,\mathrm{kV}$.

To monitor and numerically compensate for drifts, an additional reference point (with U=0 kV) is always included before and after each high-voltage deflection scan. From the interference curves thus obtained we extract the voltage dependence of the experimental fringe shift (Fig. 3). The observed fringe shift is influenced by the details of the molecular velocity distribution in three ways. Firstly, slow molecules will acquire a larger deflection in the external field gradient than fast ones (Eq. 1). Secondly, different velocity classes are associated with different visibilities. This is an important and desired feature of the Talbot-Lau arrangement, as it allows to prove the quantum wave-nature of material objects [8]. Thirdly, the van der Waals interaction with the grating walls adds a dispersive phase shift [7, 8].

The expected signal as a function of the scanning grating position x is proportional to:

$$1 + \bar{V}_{th}(\alpha)\cos\left[\frac{2\pi}{g}\left(x - \Delta s_{th}(\alpha)\right)\right]$$

$$\equiv \int \mathrm{d}v f_{\bar{v},\sigma_v}(v)\left(1 + V(v)\cos\left[\frac{2\pi}{g}\left(x - \Delta s_x(\alpha, v)\right)\right]\right) \quad (2)$$
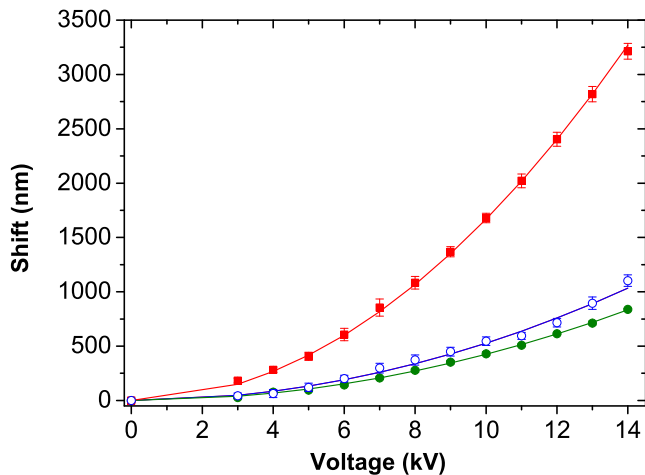
FIG. 3: The Stark-deflection of the C_{70} fringes follows precisely the quadratic voltage dependence $\Delta s \propto U^2/v^2$ of Eq. 1: full circles: $\bar{v} = 199$ m/s, $\sigma_v = 16\%$, open circles $\bar{v} = 173$ m/s, $\sigma_v = 13\%$, full squares: $\bar{v} = 109$ m/s, $\sigma_v = 7\%$.

where the velocity distribution function $f_{\bar{v},\sigma_v}(v)$ is experimentally determined for several source settings, i.e. different mean velocities $\bar{v}$. The fringe visibility function $V(v)$ cannot be measured directly because of the finite width of the velocity distribution σ_v. It is extracted from the measured visibilities $V(\bar{v}, \sigma_v)$ using

$$V(\bar{v}, \sigma_v) = \int \mathrm{d}v f_{\bar{v},\sigma_v}(v) V(v). \tag{3}$$

The polarizability α is then obtained by fitting the experimentally observed shift $\Delta s_{\exp}$ with the theoretical shift $\Delta s_{\mathrm{th}}(\alpha)$.

We limit the maximum deflection voltage in the experiment to $15\,\mathrm{kV}$ since the fringes of slow $(109\,\mathrm{m/s})$ fullerenes are then already shifted by three entire periods (Fig. 3) and dephasing effects become important. Molecules of different velocities experience a different Stark deflection, and the summation over the corresponding molecule interference patterns in the detector will reduce the total fringe visibility for sufficiently large velocity spreads σ_v and with increasing voltage (see Fig. 4). In our experiments $\sigma_v(1/e^2)$ ranges between $7\,\%$ and $16\,\%$ for molecules between $100\,\mathrm{m/s}$ and $200\,\mathrm{m/s}$, respectively.

When all grating positions are fixed, the scanning deflection voltage can be used to sweep the molecular density pattern across the third grating (Fig. 4). The data points are well described using the implicit functions of the voltage for the expected visibility $\bar{V}_{th}(\alpha)$ and shift $\Delta s_{th}(\alpha)$. It is interesting to note, that not only the shift but also the voltage dependent dephasing, which leads to a rather sharp decrease in the interference contrast, may actually be used as tools for metrology. The fringe shifts are, however, less sensitive to additional random perturbations – such as vibrations, thermal radiation or

collisions – than the visibility, and the values given below are therefore based on the displacement measurements.

We find a polarizability of $88.9 \pm 0.9 \pm 5.1\,\text{Å}^3$ for C_{60} and $108.5 \pm 2.0 \pm 6.2\,\text{Å}^3$ for C_{70}, including the statistical (first) and systematic (second) error. The relative polarizability is then $\alpha(C_{70})/\alpha(C_{60}) = 1.22 \pm 0.03$. Most of the systematic uncertainties, such as for instance field inhomogeneities, cancel out in the determination of the relative values.

The statistical uncertainty of $2\,\%$, given above, refers to the standard deviation in the determination of α for different velocities. If all data were purely shot noise limited, we would expect an uncertainty as small as $0.1\,\%$.

The uncertainty in the measurement of the velocity amounts to $1\,\%$, the voltages are known to $0.5\,\%$. The lateral resolution of our interferometer is currently good to within $\sim 15\,\mathrm{nm}$. This amounts to less than two percent of the maximum fringe shift and it corresponds to a lateral force sensitivity of better than $10^{-14}\,\mathrm{pN}$.
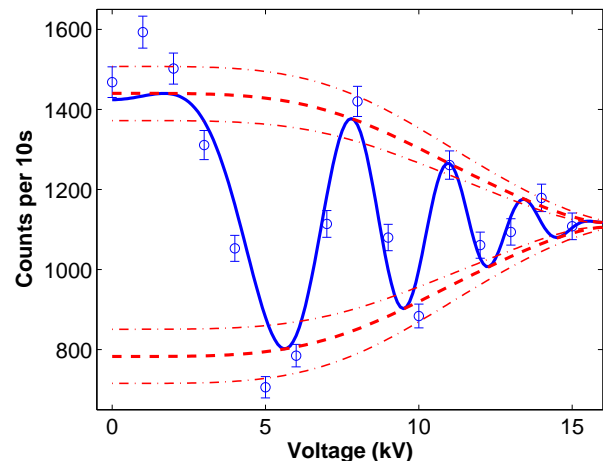

FIG. 4: Signal as a function of the deflection voltage for a fixed position of the mask grating. The open circles are data points of C_{70} at a velocity of $\bar{v} = 103.2 m/s, \sigma_v = 7\%$. The solid line is the theoretical expectation for $\alpha = 108.5\,\text{Å}^3$. The dashed line is the envelope curve of the visibility function. The dashed dotted lines illustrate upper and lower bounds resulting from small variations of the velocity distribution: $\Delta\bar{v} = \pm 1\%, \Delta\sigma_v = \pm 1\%$ and typical uncertainties of the visibility: $\Delta V(v) = \pm 3\%$.

The properties of the electric field are characterized using a finite element code [24] which finds a value of $(\mathbf{E}\nabla)E_x = (1.45 \pm 0.08) \cdot 10^{14}\,\mathrm{V}^2/\mathrm{m}^3$ for a voltage of $10\,\mathrm{kV}$. The same code is used to determine the effective electrode length $d_{\mathrm{eff}} = (4.73 \pm 0.1)\,\mathrm{cm}$ which replaces the real electrode length because of edge effects. The remaining uncertainties comprise the accuracy in the measurement of the electrode's contour and separation. All independent systematic uncertainties add up to a total of $5.7\,\%$.

In conclusion, we have demonstrated that a near-field

matter-wave interferometer is a promising tool for sensitively measuring the scalar polarizability. The three-grating design allows us to combine high spatial resolution and high molecular flux.

As mentioned before, the velocity spread is a critical parameter, since it enters quadratically in Eq. 1. However, in particular in pulsed molecular beam experiments, based on laser desorption and on pulsed photo-ionization the velocity selection can reach values as small as $\Delta v/v \sim 0.1\,\%$ at acceptable signal intensities [25], even if the entire beam has still a finite temperature. This way it is already possible to generate neutral beams of fullerenes, complex biomolecules [14, 26] up to polypeptides composed of 15 amino acids [25].

The extension of our present setup to pulsed sources and detectors is particularly interesting for instance for investigating the temperature dependence of the molecular polarizability. But also magnetic moments or triplet lifetimes of fullerenes should thus be accessible.

In biomolecules, the conformational variation of polarizabilities and electric dipole moments will be of interest. If the molecules exhibit a finite electric or magnetic dipole moment, the random orientation of cold molecules will lead to a decrease of the visibility instead of a simple fringe shift [27]. As mentioned above, the amount of dephasing will then allow the extraction of a numerical value for the moments. For hot molecular beams which possess a permanent electric dipole moment the system behaves as an object with only an induced polarizability [28]. Therefore, dipole moments could already be measured in our current setup by only replacing the source.

With respect to far-field interference methods the near-field scheme can be much extrapolated towards significantly more complex particles. And even in its classical limit, as a multiplexing Stark-deflectometer it will still combine high resolution with high transmission. Finally, it is interesting to note, that our apparatus may also be regarded as a fast switch for molecular beams. The fine-structure imprinted on the beam by its transmission through the first two gratings allows us to lower and raise the molecular transmission with kHz-frequencies. In dedicated experiments it should be possible to reach a modulation amplitude of close to 100%.

Acknowledgments

[1] K. Bonin and V. Kresin, *Electric-Dipole Polarizabilities of Atoms, Molecules and Clusters* (World Scientific, 1997), ISBN 981-02-2493-1.

[2] I. Compagnon et al., Phys. Rev. A **64**, 025201 (2001).

[3] J. A. Maddi, T. P. Dinneen, and H. Gould, Pyhsical Review A **60**, 3882 (Nov. 1999).

[4] H. L. Bethlem, G. Berden, and G. Meijer, Phys. Rev. Lett. **83**, 1558 (1999).

[5] R. Fulton, A. I. Bishop, and P. F. Barker, Phys. Rev. Lett. **93**, 243004 (2004).

[6] T. Takekoshi, J. R. Yeh, and R. J. Knize, Opt. Commun. **114**, 421 (1995).

[7] R. E. Grisenti et al., Phys. Rev. Lett. **83**, 1755 (1999).

[8] B. Brezger et al., and A. Zeilinger, Phys. Rev. Lett. **88**, 100404 (2002).

[9] K. Hornberger et al., and A. Zeilinger, Phys. Rev. Lett. **90**, 160401 (2003).

[10] P. L. Gould, G. A. Ruff, and D. E. Pritchard, Phys. Rev. Lett. **56**, 827 (1986).

[11] O. Nairz et al., Phys. Rev. Lett. **87**, 160401 (2001).

[12] B. Brezger, M. Arndt, and A. Zeilinger, J. Opt. B: Quantum Semiclass. Opt. **5**, S82 (2003).

[13] J. P. Simons et al., Intern. Rev. in Phys. Chem. **24**, 489 (2005).

[14] R. Antoine et al., J. Chem. Phys. **110**, 9771 (1999).

[15] J. M. Amini and H. Gould, Physical Review Letters **91**, 153001 (2003).

[16] C. Ekstrom et al., Phys. Rev. A **51**, 3883 (1995).

[17] A. Miffre et al., Europhysics Letters pp. 1–7 (2006).

[18] M. Arndt et al., Nature **401**, 680 (1999).

[19] K. Patorski, in *Progress in Optics XXVII*, edited by E. Wolf (Elsevier Science Publishers B. V., Amsterdam, 1989), pp. 2–108.

[20] J. Clauser and M. Reinsch, Applied Physics B **54**, 380 (1992).

[21] J. Clauser and S. Li, in *Atom Interferometry*, edited by P. R. Berman (Academic Press, 1997), vol. 11, pp. 121–151.

[22] L. Hackermüller et al., Phys. Rev. Lett. **91**, 90408 (2003).

[23] M. Arndt et al., C.R. Acad. Sci. Paris **t. 2, Série IV**, 1 (2001).

[24] *FEMLAB Reference Manual 3.0*, Comsol, Stockholm (2004).

[25] M. Marksteiner et al., Acta Phys. Hung. B **26** (2006).

[26] G. Meijer et al., Applied Physics B **51**, 395 (1990).

[27] R. Antoine et al. J. Am. Chem. Soc. **124**, 6737 (2002).

[28] R. Moro et al. Phys. Rev. Lett **97**, 123401 (2006).